Journal of Materials Chemistry C

Accepted Manuscript

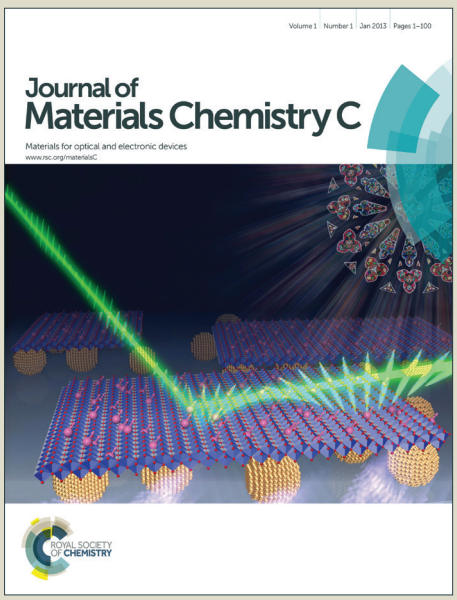

ROYAL SOCIETY OF CHEMISTRY

www.rsc.org/materialsC

Morphology and Polarization-Dependent Second Harmonic Generation in Single Hexagonal Sodium Niobate Micro/Nano-crystal

Quanlan Xiao[1], Wei Lin[1], Gengxu Chen[2], Chengjie Ding[2], Guoping Dong[1]*, Chensheng Lin[3], Botao Wu[2], E Wu[2], Heping Zeng[2] and Jianrong Qiu[1]*

[1]State Key Laboratory of Luminescent Materials and Devices and Institute of Optical Communication Materials, South China University of Technology, Guangzhou, China

[2]State Key Laboratory of Precision Spectroscopy, East China Normal University, Shanghai, China

[3]State Key Laboratory of Structural Chemistry, Fujian Institute of Research on the Structure of Mater, the Chinese Academy of Sciences, Fuzhou, China

Abstract:

We have synthesized six morphologies of $NaNbO_3$ micro/nano-crystals with three crystal structures using hydrothermal method. Each single hexagonal $NaNbO_3$ micro/nano-crystal (samples No.1-No.3) exhibits strong second-order nonlinear response. By calculating the average intensity and measuring polarization response of each single hexagonal $NaNbO_3$ micro/nano-crystal (samples No.1-No.3), it has demonstrated that the same crystal structure displays a similar optical second harmonic generation (SHG) response, furthermore, SHG is independent of the morphology and identical for similar crystals, which is expected for a volume effect with a second-order susceptibility tensor depending on the material properties. Based on the previous related research and the optical SHG properties of $NaNbO_3$ micro/nano-crystals, the non-toxic $NaNbO_3$ micro/nano-crystals may find promising applications in biological imaging, etc.

Keywords: Sodium Niobate; Micro/Nano-crystals; Second Harmonic Generation; Morphology; Polarization

* Author to whom correspondence should be addressed. E-mail address: dgp@scut.edu.cn, qjr@scut.edu.cn.

1 Introduction

Second harmonic generation (SHG) is a second-order nonlinear optical process, where two photons are combined and converted into a single photon with twice the fundamental frequency, and is particularly interesting because it is only efficient in noncentrosymmetric environments---most typically an inorganic crystal.[1, 2] By oversimplifying, we can explain this property as the absence of symmetry on a microscopic scale. As a matter of fact, SHG can be observed at interfaces and some biological materials because these materials can be highly polarizable and often assemble into large, ordered noncentrosymmetric structures. For example, cell membranes, where a sudden change occurs in the optical properties of the medium going from the inside to the outside of a cell;[2] and elongated structure as collagen (and not isotropic), which can produce SHG signals due biological membranes might be good general scaffolds for noncentrosymmetric arrays of SHG-active molecules.[3] Therefore, for SHG coming from exogenous nanoparticles, which provide high contrast in unstructured and isotropic environments. For endogenous SHG (intrinsic structures directly produce strong SHG), labeling with exogenous molecular probes is not required.

Recently, SHG studies of nanomaterials have become a very active field. And SHG process has been observed from different types of nanomaterials, including metals,[4-6] semiconductor,[7-12] organic nanomaterials,[13-15] dielectric.[16-21] Unlike photoluminescence, the SHG process occurs without nonradiative energy loss and involves only virtual electron energy transition; therefore SHG structures do not bleach over time and emit a stable, nonblinking signal that does not saturate with increasing excitation power.[12, 22-23] Furthermore, SHG is generally a nonresonant process that offers flexibility of tuning the wavelength of the SHG signal by changing the excitation wavelength accordingly.[20] Since the SHG conversion efficiency of these nanomaterials is sufficiently high, it has shown great potential as alternative imaging probes due to their non-bleaching and non-blinking signal as well as the advantages of stable, tunable, coherent, fast, polarization sensitive.[1-2, 7, 16, 19-21, 23-28] Due to their unique optical properties, these SHG nanoprobes offer opportunities that are not available with

photoluminescent probes. Besides, SHG has proven to be a very useful tool in optics and materials characterization, it has been extensively used as an analytical tool for monitoring surfaces, interfaces, and ferromagnetic domain growth.

Since SHG only takes place in a noncentrosymmetric environment under electric dipole approximation,[1] nanomaterials of noncentrosymmetric crystal structures are efficient in SHG. The SHG process of various noncentrosymmetric nanocrystals has been studied, which includes ZnO,[9-12] $KTiOPO_4$ (KTP),[16, 18, 24] $Fe(IO_3)_3$,[19, 22] GaAs,[26] $XNbO_3$ (X = Li, Na, K),[20, 29] $BaTiO_3$,[21, 25, 31-32] etc. Herein, we study the SHG responses from single hexagonal $NaNbO_3$ micro/nano-crystals with different morphologies and sizes (samples No.1-No.3). The calculated average intensity and the measured polarization dependence of each single hexagonal particle (samples No.1-No.3) are studied in detail. Through these studies, we are able to find the influence factors of SHG response and polarization and how the SHG responses depend on the impinging light polarization. Furthermore, from the measured polarization dependence of a micro/nano-crystal, we are also able to find the orientation of the micro/nano-crystal. Motivated by the advantages of SHG imaging probes (such as stable, tunable, coherent, fast, polarization sensitive, etc.) and no toxicity of $NaNbO_3$ crystals, the as-prepared $NaNbO_3$ micro/nano-crystals open up the possibilities in biological imaging.

2 Experimental

2.1 Materials synthesis

In this work, the $NaNbO_3$ micro/nano-crystals are produced by a two-step hydrothermal method. First, a metastable potassium niobate precursor is prepared by a hydrothermal process. Then, the mixture of the solid potassium niobate precursor and NaOH solution (pure water, ethylene glycol/water, or ethylenediamine/water) are followed by the ion exchange reaction under hydrothermal conditions. The resulting powders are washed several times with distilled water and then dried at room temperature. (For the details, please see the experimental section

in Supplementary). The flowchart is shown in Supplementary Fig. S1 and the experimental parameters of as-prepared $NaNbO_3$ micro/nano-crystals are shown in Supplementary Table S1.

2.2 Characterization methods

The crystal structure and phase purity of as-prepared samples are investigated by X-ray diffraction (XRD) (Bruker, D8 ADVANCE analysis with Cu Kα radiation operated at 40 kV and 40 mA, λ = 0.15418 nm, scanning step 0.02°, scanning speed 0.1 s per step). The morphology, structure and size distribution of the powders are observed by transmission electron microscope (TEM, JEM-100CXⅡ) and field emission-scanning electron microscopy (FE-SEM, Nova NanoSEM430, FEI, Netherlands). SEM equipped with an energy-dispersive X-ray spectrometer (EDS) is used to study the composition of powders. To further determine the structure and phase of nanocrystals, high-resolution transmission electron microscopy (HR-TEM) images and selected area electron diffraction (SAED) patterns are performed using transmission electron microscope (TEM, JEM-100CXⅡ). For the nonlinear optical second-harmonic generation (SHG) measurement of single $NaNbO_3$ particles, we use a combined system of a scanning confocal microscope and an atomic force microscope (AFM). A home-built Yb-doped fiber laser with 1064 nm, 30 MHz, 11 ps is used as an excitation beam. The incident beam propagates first through a polarizer which makes it becoming a linear polarized source. Then it goes through a half-wave plate which allows varying the angle of the polarization. Afterward, the beam is focused to 927 nm in diameter by an oil-immersion objective (×100, numerical aperture (N.A.) = 1.40, oil immersion, Olympus UPlanSApo) onto the sample plane, and the emission of SHG occurs. The emitted SHG light and the incident light are then collected by the same microscope objective. The path of both beams is separated by a dichroic mirror after the objective. It transmits the SHG light and reflects most of the incident light. After passing through dichroic mirror, the small amount of the incident beam is still transmitted, and is filtered out by a band pass filter at 532 nm with bandwidth of 3 nm. And the beam is also spatially filtered by a pinhole with diameter of 75 um in a telescope system. The SHG signal is detected by single-photon detector based on Si-avalanche photodiode (APD). The sample of the

coverslip with $NaNbO_3$ micro/nano-crystals is held on an *x-y* piezo stage. By scanning the piezo stage, the confocal images of the single $NaNbO_3$ micro/nano-crystals can be obtained. On the top of the scanning confocal microscope, an AFM (NanoWizard Ⅱ, JPK) is installed to acquire the surface topography of the nanocrystal. The tip of the AFM is aligned coaxially with the confocal microscope. Schematic of the optical SHG measurements setup is shown in Fig. 1. All the measurements are investigated at room temperature.

3 Results and discussion

The $NaNbO_3$ micro/nano-crystals are synthesized by hydrothermal method. $NaNbO_3$ micro/nano-crystals with six different morphologies and three types of crystal structures have been successfully fabricated through controlling the synthesis conditions, such as the surfactant and reaction medium (pure water, ethylene glycol/water, ethylenediamine/water). The relevant details show in Supplementary.

3.1 Phases, structures, morphologies and sizes

The XRD patterns of as-prepared $NaNbO_3$ micro/nano-crystals (sample No.1 to No.6) are given in Fig. 2, and the interrelated SEM, TEM, HR-TEM and SAED images are shown in Supplementary Fig. S4. Fig. 2 has confirmed that all the samples are $NaNbO_3$, the samples No.1-No.3 and No.5 present the pure hexagonal phase $NaNbO_3$ (Joint Committee on Powder Diffraction Standards (JCPDS) Card No. 37-1076, space group: *R*, $a = b =$ 0.5335 nm, $c = 1.5611$ nm), sample No.1 is nanowire with ~270 nm in width and ~25 μm in length, sample No.2 is a regular hexagonal microplate with a size of ~ 6 μm, sample No.3 are irregular cubic nanoparticles with a size of ~ 60 nm, and sample No.5 is nanorod with ~360 nm in width and ~8 μm in length. The sample No.4 presents the pure cubic phase $NaNbO_3$ ($K_2Ta_2O_6$: JCPDS Card No. 35-1464, space group: *Fd-3m*, $a = b = c = 1.0596$ nm) and irregular polyhedral nanoparticle with a size of ~ 2.5 μm is obtained. The XRD pattern of the sample No.4 indicates that these diffraction peaks are consistent with cubic $K_2Ta_2O_6$. The EDS data exhibits the presence of Na, Nb, and O elements, and no other elements can be detected (see Supplementary Fig. S5). The sample No.6

presents pure cubic phase $NaNbO_3$ (JCPDS Card No. 75-2102, space group: *Pm-3m*, $a = b = c = 0.3906$ nm) and regular cubic nanoparticle with a size of ~ 630 nm is obtained. Their structures all exhibit a complicated three-dimensional (3D) network composed of NbO_6 (NbO_8) distorted polyhedra as shown in Fig. 2d, e and f, respectively. For samples No.1-No.3 and No.5 shown in Fig. 2g, in a NbO_6 octahedron, the Nb-$O_{1(2, 3)}$ distances of 2.1123Å are all longer than the corresponding distances Nb-$O_{4(5, 6)}$ of 1.8886Å, and Nb^{5+} cation displacement is along the three-fold rotational axis of the octahedron that passes through the triangle faces $O_1O_2O_3$ and $O_4O_5O_6$, this displacement of the cation leads to the loss of a symmetrical center of NbO_6 polyhedra, and lots of NbO_6 polyhedra are interconnected via a sharing corner into a 3D framework. For sample No.4, in a NbO_8 octahedron shown in Fig. 2h, the Nb-$O_{1(2, 4)}$ and Nb-O_3 distances of 2.6595Å and 1.9530Å are consistent with the corresponding Nb-$O_{5(6, 8)}$ and Nb-O_7 distances of 2.6195Å and 1.9530Å, and Nb^{5+} cation displacement is along the four-fold rotational axis of the octahedron that passes through the triangle faces $O_1O_2O_3O_4$ and $O_5O_6O_7O_8$, NbO_8 polyhedra is a structure with symmetrical center, then further interconnecting into a 3D framework. For sample No.6, the Nb-$O_{1(2, 3, 4, 5, 6)}$ distances of 1.9530Å are all the same in a NbO_6 octahedron with a symmetrical center, then further interconnecting into a 3D framework, as shown in Fig. 2i. The kinds of phases, structures, specific sizes and morphologies of $NaNbO_3$ micro/nano-crystals prepared with different preparation conditions are quite different, and the growth mechanism of the samples is discussed as shown in Supplementary Fig. S6.

The phases, structures, morphologies and sizes of as-prepared $NaNbO_3$ micro/nano-crystals could be clearly seen in Table 1. Considering the SHG is effective in noncentrosymmetric crystal structures of micro/nano-materials and may be different in various morphologies, we study the optical SHG of single hexagonal $NaNbO_3$ micro/nano-crystals (samples No.1-No.3) in detail in the following.

3.2 Optical SHG of single hexagonal $NaNbO_3$ micro/nano-crystals (samples No.1-No.3)

Fig. 3 shows the SHG images (left column) of each single hexagonal $NaNbO_3$ micro/nano-crystal (samples No.1-No.3) with different morphologies and sizes, and their corresponding CCD or AFM images (right columns),

which are used to determine the respective morphologies and ensure that the SHG responses are from single hexagonal particles. Sample No.3 exhibits a relative weak response due to its small size, so we probe optical SHG response in several nanoparticles of sample No.3. All the hexagonal $NaNbO_3$ micro/nano-crystals (samples No.1-No.3) exhibit strong nonlinear SHG responses. In order to compare SHG responses of each single hexagonal $NaNbO_3$ micro/nano-crystal, we calculate the average intensity of SHG responses for each single hexagonal $NaNbO_3$ micro/nano-crystal (samples No.1-No.3) as shown in Fig. 4. The average intensity is estimated through the calculation of SHG response intensity on unit volume in each single hexagonal $NaNbO_3$ micro/nano-crystal (samples No.1-No.3) and the running power is fixed as 10 mW. Since the crystallinity of the sample No.3 is a bit poor, its SHG response is a little weaker than that of the samples No.1 and 2, but there are no significant differences in the average intensity of SHG responses among these various single hexagonal $NaNbO_3$ crystals. The samples No.1-No.3 display the similar average intensity of SHG responses, therefore, it can be deduced that the morphology and size have no significant effect on the average intensity of SHG response of single hexagonal $NaNbO_3$ micro/nano-crystals (samples No.1-No.3). Furthermore, SHG coming from the same crystal structure is independent of the morphology, while the size is larger, the SHG response intensity is stronger due to the volume effect.

3.3 Power dependency measurements of single hexagonal $NaNbO_3$ micro/nano-crystals (samples No.1-No.3)

In order to ensure that the detected response is indeed from the SHG process, power dependency measurements are also conducted for each single hexagonal $NaNbO_3$ micro/nano-crystal (samples No.1-No.3), red curves are the SHG power responses quadratic fitting the measurements (blue dots) (Fig. 5). Because the SHG intensities of sample No.1 and No.2 are very strong, the running excitation powers of sample No.1 and No.2 are set under 20 mW to avoid the damage of detector during the test. Therefore, more than half of the plots for sample No.1 and No.2 do not have measurement points in Fig. 5, but this will not affect the experimental results. All the hexagonal $NaNbO_3$ micro/nano-crystals (samples No.1-No.3) show a typical quadratic behavior, indicating that

the responses are generated from a second order nonlinear process. Besides, in the experimental data of Fig. 5, it shows that no saturation effect occurs with increasing excitation power.

3.4 Polarization dependence measurements of single hexagonal $NaNbO_3$ micro/nano-crystals (samples No.1-No.3)

We perform polarization-dependent measurements on each single hexagonal $NaNbO_3$ micro/nano-crystal (samples No.1-No.3) in order to study the polarization dependence of SHG responses, which include the impinging light polarization and the influence factors of polarization. The optical *c*-axis lies along the light propagation (Z-axis of our coordinate system as shown in Fig. 6). A change of the orientation between the polarization of the incident light and the *c*-axis of coordinate system generates a different amount of SHG response. In other words, the SHG response can be determined only by the orientation of the *c*-axis, which is related to the laboratory frame (x, y, z) by three Euler angles $\Omega(\psi,\theta,\varphi)$ in Euler coordinate, as depicted in Fig. 6. The incident light is assumed in the *x*-*y* plane and acting on the crystal, which propagates along the *Z*-axis and the excitation polarization angle γ can be rotated in the *x*-*y* plane by a half-wave plate having electric field components E_x and E_y. This incident field defined in normal Cartesian coordinates system has to be first projected onto the crystal coordinate system (x', y', z'). After the conversion of the coordinate system, the SHG polarization can be calculated by simply using the second-order polarization:[7, 32]

$$\vec{P}(2\omega) = \varepsilon_0 \chi^{(2)} \vec{E}(\omega)^2 \quad (1)$$

where ε_0 is the permittivity of the free space, $\chi^{(2)}$ is the coefficients of the second-order susceptibility tensor, *E* is the incident field, and ω is the frequency of the incident light. In the simulation, along with the experimental points is displayed the curve adjusted with the following expression of the SHG intensity:

$$I = a*\cos^4\gamma + b*\cos^2\gamma\sin^2\gamma + c\sin^4\gamma + d\cos^3\gamma\sin\gamma + e\cos\gamma\sin^3\gamma \quad (2)$$

where the different parameters *a*, *b*, *c*, *d*, and *e* can be related to the Euler angles $\Omega(\psi,\theta,\varphi)$, the related derivation shows in Supplementary Part 7.

The calculated band gap of $NaNbO_3$ (JCPDS Card No. 37-1076, space group: *R*) is 3.714 eV by using Heyd-Scuseria-Ernzerhof (HSE) method in the code of CASTEP. The dielectric function can be calculated from the first-order susceptibility and linear refractive index. The first-order non-resonant susceptibility at low frequency region is given by $\chi^{(1)}(\omega)_{ii} = [\varepsilon(\omega)_{ii} - 1]/4\pi$, and the linear refractive index $[n(\omega \to 0)]_{ii}^2 = \varepsilon_1(\omega \to 0)_{ii}$. The second-order susceptibilities can be expressed in terms of the first-order susceptibilities as follows:[33, 34]

$$\chi_{ijk}^{(2)} = (-\omega_3; \omega_1, \omega_2) = F^{(2)} \chi_{ii}^{(1)}(\omega_3) \chi_{jj}^{(1)}(\omega_1) \chi_{kk}^{(1)}(\omega_2) \quad (3)$$

Where $F^{(2)} = ma/(N^2 e^3)$. These expressions are derived from a classical anharmonic oscillator (AHO) model. The *m* and *e* are respectively the electron mass and charge, and the parameter *a*, which characterizes the nonlinearity of the response, can be obtained from experimental or theoretical estimations. In this calculation, the *F* factor is estimated to be 1.124.

Under the restriction of Kleinman's symmetry, only three independent SHG tensor components (d_{22}, d_{31}, and d_{33}) are considered. The calculated three frequency-dependent nonlinear optical (NLO) components (d_{22}, d_{31}, and d_{33}) of the $NaNbO_3$ are plotted in Fig. 7. The calculated tensor coefficients of bulk $NaNbO_3$ (JCPDS Card No. 37-1076, space group: *R*) are d_{22} = 17.3 pm/V, d_{31} = 16.0 pm/V, and d_{33} = 14.2 pm/V at a wavelength of 1064 nm (1.165 eV), respectively.

Fig. 8 shows the SHG polarization analysis for the single hexagonal $NaNbO_3$ micro/nano-crystals (samples No.1-No.3). The responses of samples No.1-No.3 all display two leaves, which have nonzero diagonal elements in the second-order susceptibility tensor, exhibit a dipolar emission pattern corresponding very often to two lobes for one analysis orientation. Therefore, we can conclude that the morphology and size have no significant effect on the polarization property of SHG responses. This result is agreement with the calculation of the average intensity for each single hexagonal $NaNbO_3$ particle (samples No.1-No.3). Moreover, the simulation also reveals the information on the orientation of each single hexagonal $NaNbO_3$ particle (samples No.1-No.3) defined by

$\Omega(\psi,\theta,\varphi)$, which are (52.3°, 110.6°, 82.5°) for sample No.1, (55.8°, 106.1°, 80.7°) for sample No.2, and (67°, 111.4°, 76.8°) for sample No.3. Motivated by the advantages of SHG imaging probes (such as stable, tunable, coherent, fast, polarization sensitive, etc.),[1-2, 7, 16, 19-21, 23-28] some recent work have reported that nonlinear materials have been applied in biological imaging. For example, Culic-Viskota et al.[35] have studied $BaTiO_3$ SHG nanoprobes for in vivo imaging in living zebra fish embryos resulting that the signal to noise ratio (SNR) is greatly improved. Similarly, $KNbO_3$ nonlinear nanoparticles are used to monitor the evolution of embryonic stem cell (ESC) by second harmonic microscopy has been studied by Magouroux et al.[36], and so on. Therefore, based on the previous related research and the optical SHG properties of $NaNbO_3$ micro/nano-crystals, the non-toxic $NaNbO_3$ micro/nano-crystals may find promising applications in biological imaging.

4 Conclusions

We prepare six morphologies of $NaNbO_3$ micro/nano-crystals with three crystal structures using hydrothermal method. The optical SHG from single hexagonal $NaNbO_3$ micro/nano-crystals (samples No.1-No.3) with different morphologies and sizes is studied. Each single hexagonal particle in samples No.1-No.3 shows a typical quadratic dependency of the SHG with the incident beam power, showing that the response is generated from a second-order nonlinear process. Moreover, by calculating the average intensity of the SHG response for each single hexagonal $NaNbO_3$ micro/nano-crystal (samples No.1-No.3), showing that SHG is independent of the morphology and identical for similar crystals, which is expected for a volume effect with a second-order susceptibility tensor depending on the material properties. By measuring the polarization of the SHG response for each single $NaNbO_3$ micro/nano-crystal (samples No.1-No.3), we can conclude that the morphology and size have no significant effect on the polarization property of SHG responses. The as-prepared $NaNbO_3$ micro/nano-crystals open up the possibilities in biological imaging based on the previous related research and the optical SHG properties of $NaNbO_3$ micro/nano-particles.

Acknowledgements

This work has been supported by the National Natural Science Foundation of China (Grant NO. 51132004, 51072054, 61475047), Natural Science Foundation of Guangdong Province (Grant NO. S2011030001349), the Guangdong Natural Science Foundation for Distinguished Young Scholars (2014A030306045), the Pearl River S&T Nova Program of Guangzhou (2014J2200083).

References

[1] R. W. Boyd, Academic Press: New York, 1992, 41.

[2] L. Bonacina, Mol. Pharmaceutics, 2013, **10**, 783.

[3] P. J. Campagnola and L. M. Loew, Nat. Biotechnol, 2003, **21**, 1356.

[4] J. I. Dadap, J. Shan, K. B. Eisenthal and T. F. Heinz, Phys. Rev. Lett., 1999, **83**, 4045.

[5] J. Nappa, G. Revillod, A. I. Russier, E. Benichou, C. Jonin and P. F. Brevet, Phys. Rev. B, 2005, **71**, 165407.

[6] J. Butet, J. Duboisset, G. Bachelier, A. I. Russier, E. Benichou, C. Jonin and P. F. Brevet, Nano Lett., 2010, **10**, 1717.

[7] M. Zielinski, D. Oron, D. Chauvat and J. Zyss, Small, 2009, **5**, 2835.

[8] M. Jacobsohn and U. Banin, J. Phys. Chem. B, 2000, **104**, 1.

[9] J. C. Johnson, H. Q. Yan, R. D. Schaller, P. B. Petersen, P. D. Yang and R. J. Saykally, Nano Lett., 2002, **2**, 279.

[10] S. W. Chan, R. Barille, J. M. Nunzi, K. H. Tam, Y. H. Leung, W. K. Chan and A. B. Djurisic, Appl. Phys. B-Lasers Opt., 2006, **84**, 351.

[11] A. V. Kachynski, A. N. Kuzmin, M. Nyk, I. Roy and P. N. Prasad, J. Phys. Chem. C, 2008, **112**, 10721.

[12] T. R. Kuo, C. L. Wu, C. T. Hsu, W. Lo, S. J. Chiang, S. J. Lin, C. Y. Dong and C. C. Chen, Biomaterials, 2009, **30**, 3002.

[13] Y. Z. Shen, P. Markowicz, J. Winiarz, J. Swiatkiewicz and P. N. Prasad, Opt. Lett., 2001, **26**, 725.

[14] S. Brasselet, L. V. Floch, F. Treussart, J. F. Roch, J. Zyss, A. E. Botzung and A. Ibanez, Phys. Rev. Lett., 2004, **92**, 207401.

[15] E. Delahaye, N. Tancrez, T. Yi, I. Ledoux, J. Zyss, S. Brasselet and R. Clement, Chem. Phys. Lett., 2006, **429**, 533.

[16] L. L. Xuan, C. Zhou, A. Slablab, D. Chauvat, C. Tard, S. Perruchas, T. Gacoin, P. Villeval and J. F. Roch,

Small, 2008, **4**, 1332.

[17] E. M. Rodriguez, A. Speghini, F. Piccinelli, L. Nodari, M. Bettinelli, D. Jaque and J. G. Sole, J. Physi. D-Appl. Phys., 2009, **42**, 102003.

[18] P. Wnuk, L. L. Xuan, A. Slablab, C. Tard, S. Perruchas, T. Gacoin, J. F. Roch, D. Chauvat and C. Radzewicz, Opt. Express, 2009, **17**, 4652.

[19] L. Bonacina, Y. Mugnier, F. Courvoisier, L. R. Dantec, J. Extermann, Y. Lambert, V. Boutou, C. Galez and J. P. Wolf, Appl. Phys. B-Lasers Opt., 2007, **87**, 399.

[20] Y. Nakayama, P. J. Pauzauskie, A. Radenovic, R. M. Onorato, R. J. Saykally, J. Liphardt and P. D. Yang, Nature, 2007, **447**, 1098.

[21] C. L. Hsieh, Y. Pu, R. Grange and D. Psaltis, Opt. Express, 2010, **18**, 11917.

[22] J. Extermann, L. Bonacina, E. Cuna, C. Kasparian, Y. Mugnier, T. Feurer and J. P. Wolf, Opt. Express, 2009, **17**, 15342.

[23] P. Pantazis, J. Maloney, D. Wu and S. E. Fraser, Proc. Natl. Acad. Sci. U. S. A., 2010, **107**, 14535.

[24] L. L. Xuan, S. Brasselet, F. Treussart, J. F. Roch, F. Marquier, D. Chauvat, S. Perruchas, C. Tard and T. Gacoin, Appl. Phys. Lett., 2006, **89**, 121118.

[25] C. Fang, D. Zhou and S. Gong, Phys. B, 2011, **406**, 1317.

[26] R. Grange, G. Brönstrup, M. Kiometzis, A. Sergeyev, J. Richter, C. Leiterer, W. Fritzsche, C. Gutsche, A. Lysov and W. Prost, Nano Lett., 2012, **12**, 5412.

[27] C. L. Hsieh, Y. Pu, R. Grange, G. Laporte and D. Psaltis, Opt. Express, 2010, **18**, 20723.

[28] D. Staedler, T. Magouroux, R. Hadji, C. Joulaud, J. Extermann, S. Schwung, S. Passemard, C. Kasparian, G. Clarke and M. Gerrmann, ACS Nano, 2012, **6**, 2542.

[29] F. Dutto, C. Raillon, K. Schenk and A. Radenovic, Nano Lett., 2011, **11**, 2517.

[30] Y. Pu, R. Grange, C. L. Hsieh and D. Psaltis, Phys. Rev. Lett., 2010, **104**, 207402.

[31] J. F. Lomax, J. J. Fontanella, C. A. Edmondson, M. C. Wintersgill, M. A. Westgate and S. Eker, J. Phys. Chem. C, 2012, **116**, 23742.

[32] E. Kim, A. Steinbrück, M. T. Buscaglia, V. Buscaglia, T. Pertsch and R. Grange, ACS Nano, 2013, **7**, 5343.

[33] R. W. Boyd, Academic Press: New York, 1992, 21.

[34] W. L. Zhang, W. D. Cheng, H. Zhang, L. Geng, C. S. Lin and Z. Z. He, J. Am. Chem. Soc., 2010, **132**, 1508.

[35] J. Culic-Viskota, W. P. Dempsey, S. E. Fraser and P. Pantazis, Nat. Protoc., 2012, **7**, 1618.

[36] T. Magouroux, J. Extermann, P. Hoffmann, Y. Mugnier, R. L. Dantec, M. E. Jaconi, C. Kasparian, D. Ciepielewski, L. Bonacina and J. P. Wolf, Small, 2012, **8**, 2752.

Figure captions

Fig. 1 Schematic of the optical SHG measurements setup. HWP is the half-wave plate. APD is the Si-avalanche photodiode.

Fig. 2 (a, b, c) XRD patterns of all samples. (d) lattice cell of $NaNbO_3$ (JCPDS Card No. 37-1076) for samples No.1-No.3 and No.5 viewed along axis *c*. (e) lattice cell of $NaNbO_3$ ($K_2Ta_2O_6$ JCPDS Card No. 35-1464) for samples No.4 viewed along axis *c*. (f) four cells of $NaNbO_3$ (JCPDS Card No. 75-2102) for samples No.6 viewed along axis *b*. (g, h, i) bond lengths of Nb-O in octahedral [NbO_6] or [NbO_8] structure. Wine ball: Nb and red ball: O.

Fig. 3 SHG images (left column) and corresponding CCD or AFM images (right column) of single hexagonal $NaNbO_3$ micro/nano-crystals (samples No.1-No.3) with different structures and morphologies.

Fig. 4 The average intensity of SHG response on unit volume for each single hexagonal $NaNbO_3$ micro/nano-crystal (samples No.1-No.3), which is estimated through the calculation of SHG response intensity on unit volume and the running power is fixed as 10 mW.

Fig. 5 SHG power dependency of single hexagonal $NaNbO_3$ micro/nano-crystals (samples No.1-No.3). The blue dots are the experimental results of measured SHG intensity, and the red curves are the quadratic fitting results.

Fig. 6 Schematic of experimental geometry employed for polarization experiments on the single hexagonal $NaNbO_3$ micro/nano-crystals (samples No.1-No.3).

Fig. 7 The calculated frequency-dependent SHG coefficients of bulk $NaNbO_3$ (JCPDS Card No. 37-1076, space group: *R*).

Fig. 8 Polarization dependence of the SHG responses from single hexagonal $NaNbO_3$ micro/nano-crystals (samples No.1-No.3), red curves are the SHG polarizaton responses fitting the measurements (blue dots). All units are in degrees.

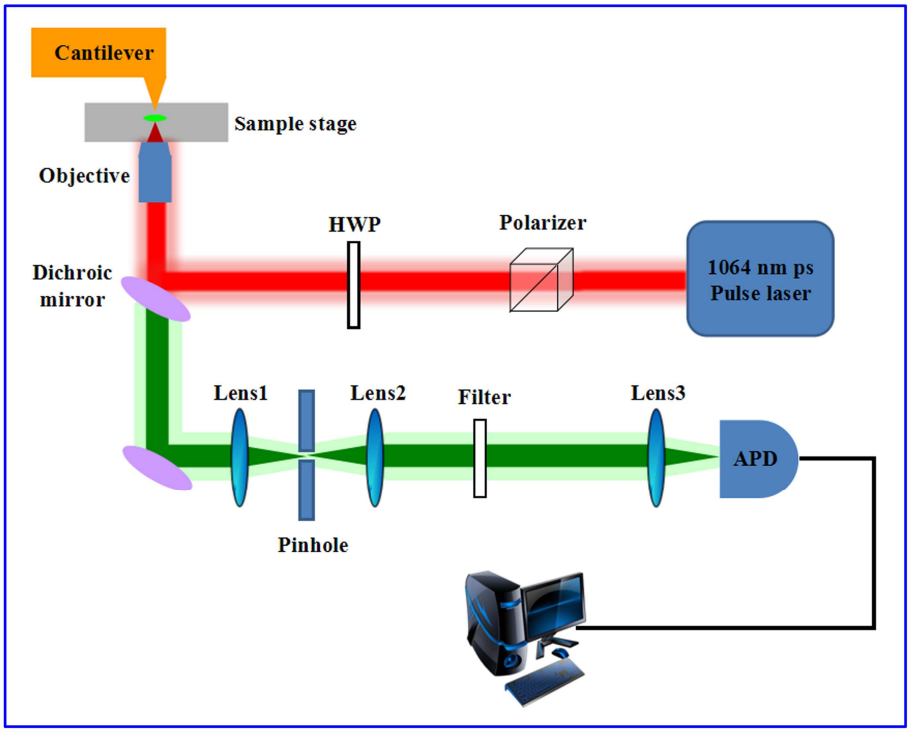

Fig. 1 Schematic of the optical SHG measurements setup. HWP is the half-wave plate. APD is the Si-avalanche photodiode.

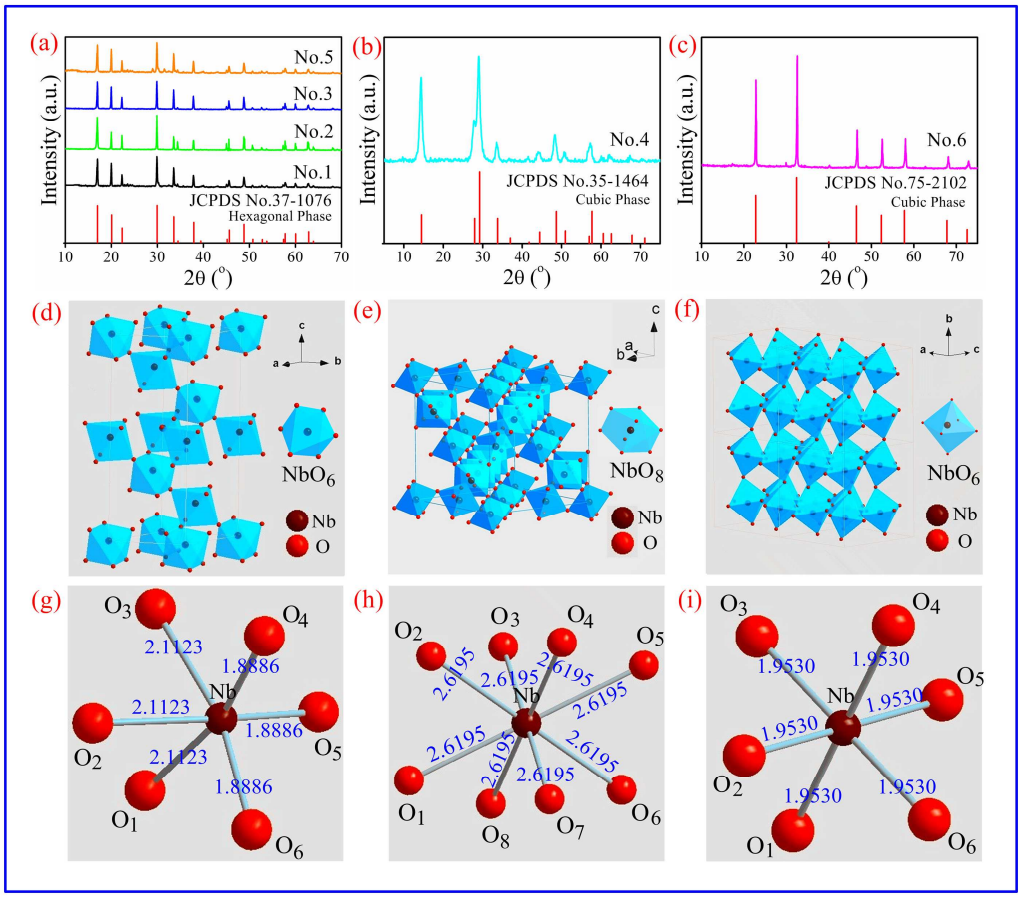

Fig. 2 (a, b, c) XRD patterns of all samples. (d) lattice cell of $NaNbO_3$ (JCPDS Card No. 37-1076) for samples No.1-No.3 and No.5 viewed along axis *c*. (e) lattice cell of $NaNbO_3$ ($K_2Ta_2O_6$ JCPDS Card No. 35-1464) for samples No.4 viewed along axis *c*. (f) four cells of $NaNbO_3$ (JCPDS Card No. 75-2102) for samples No.6 viewed along axis *b*. (g, h, i) bond lengths of Nb-O in octahedral [NbO_6] or [NbO_8] structure. Wine ball: Nb and red ball: O.

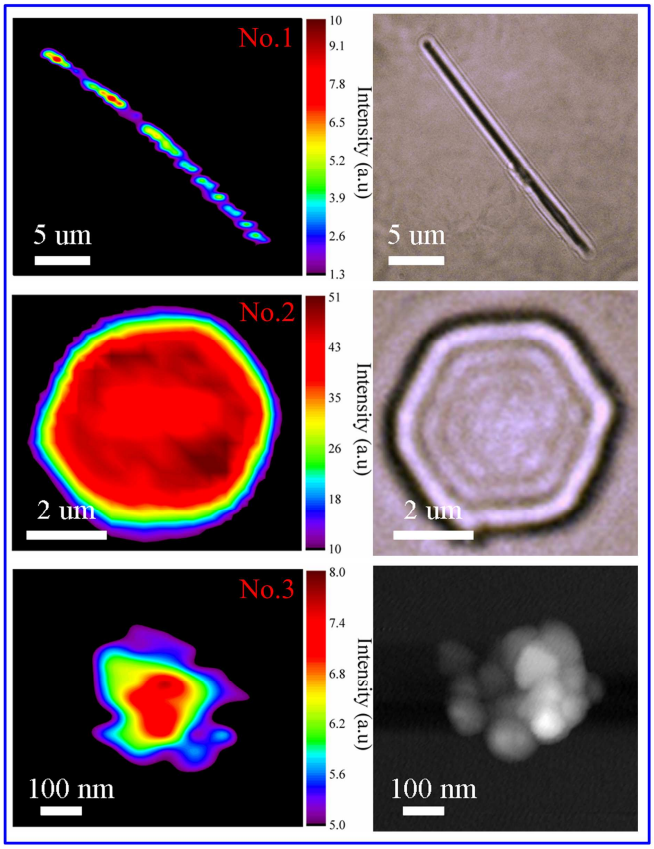

Fig. 3 SHG images (left column) and corresponding CCD or AFM images (right column) of single hexagonal $NaNbO_3$ micro/nano-crystals (samples No.1-No.3) with different structures and morphologies.

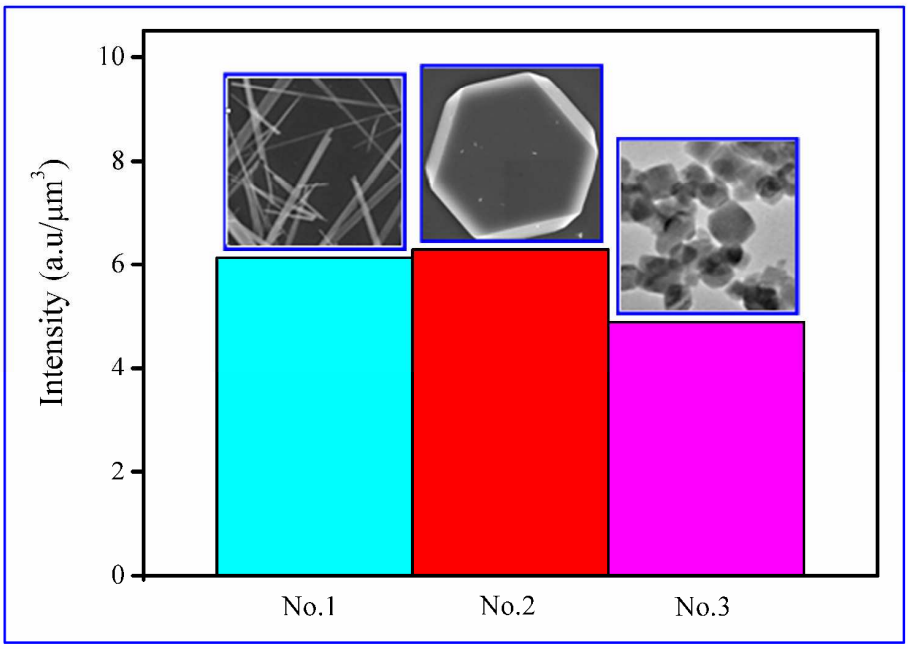

Fig. 4 The average intensity of SHG response on unit volume for each single hexagonal $NaNbO_3$ micro/nano-crystal (samples No.1-No.3), which is estimated through the calculation of SHG response intensity on unit volume and the running power is fixed as 10 mW.

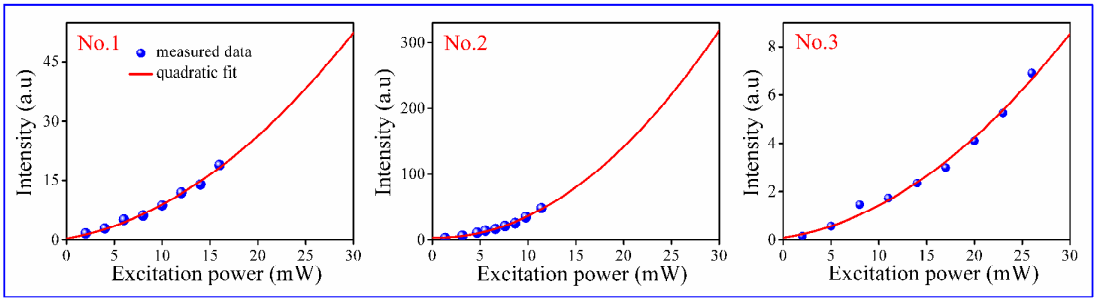

Fig. 5 SHG power dependency of single hexagonal $NaNbO_3$ micro/nano-crystals (samples No.1-No.3). The blue dots are the experimental results of measured SHG intensity, and the red curves are the quadratic fitting results.

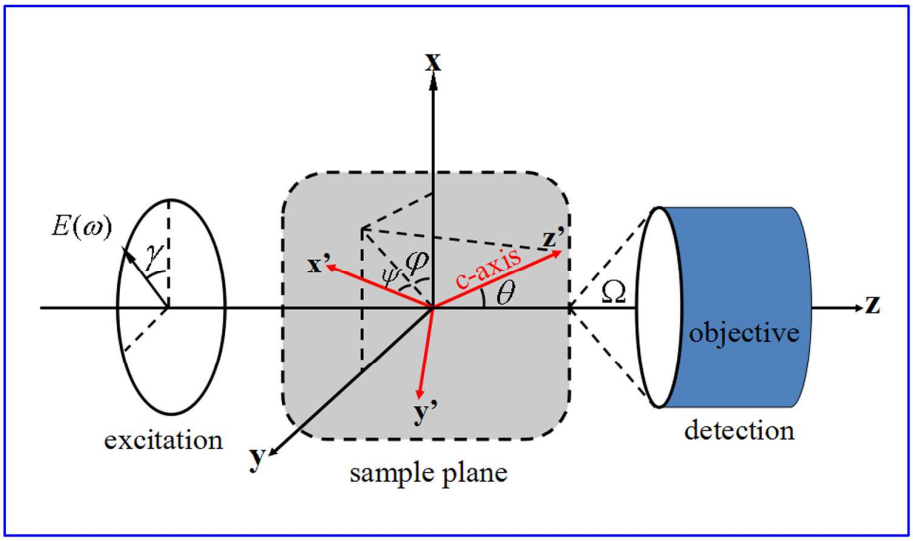

Fig. 6 Schematic of experimental geometry employed for polarization experiments on the single hexagonal $NaNbO_3$ micro/nano-crystals (samples No.1-No.3).

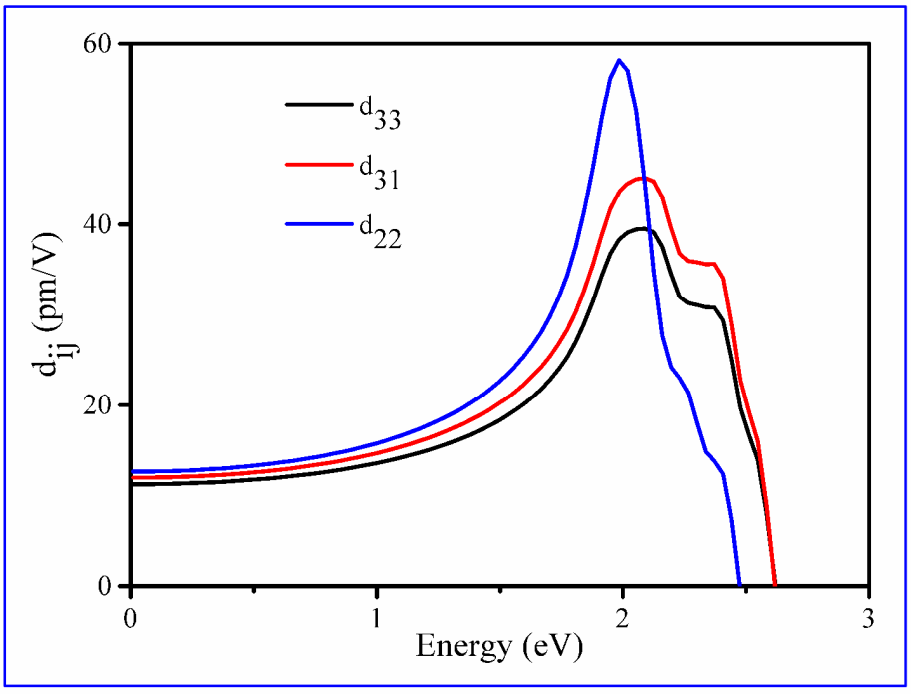

Fig. 7 The calculated frequency-dependent SHG coefficients of bulk $NaNbO_3$ (JCPDS Card No. 37-1076, space group: *R*).

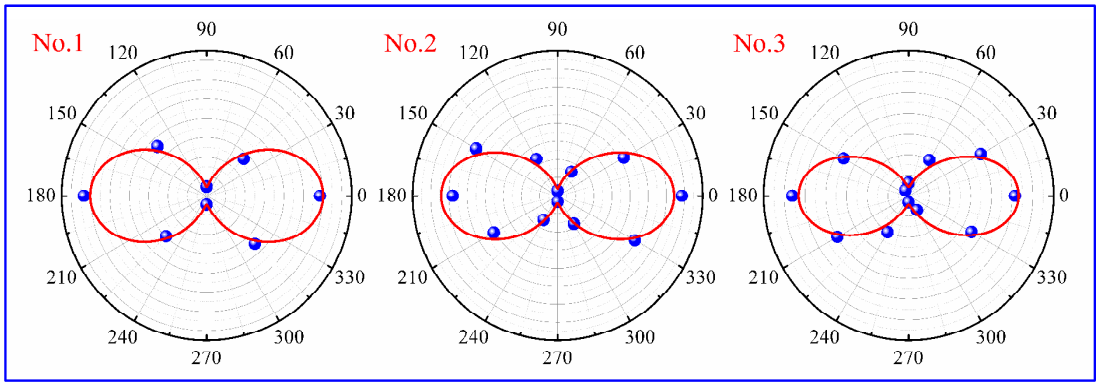

Fig. 8 Polarization dependence of the SHG responses from single hexagonal $NaNbO_3$ micro/nano-crystals (samples No.1-No.3), red curves are the SHG polarizaton responses fitting the measurements (blue dots). All units are in degrees.

Table 1 Phases, structures, morphologies and sizes of as-prepared $NaNbO_3$ micro/nano-crystals.

Sample No.	Phase	Space group	Morphology	Size
No.1	hexagonal	*R*		width ~270 nm length ~25 μm
No.2	hexagonal	*R*		~ 6 μm
No.3	hexagonal	*R*		~ 60 nm
No.4	cubic	*Fd-3m*		~ 2.5 μm
No.5	hexagonal	*R*		width ~360 nm length ~8 μm
No.6	cubic	*Pm-3m*		~ 630 nm

Graphical Abstract

The SHG responses from single hexagonal $NaNbO_3$ micro/nano-crystals with different morphologies and sizes were studied in detail. By calculating the average intensity and measuring polarization response of each hexagonal $NaNbO_3$ micro/nano-crystal, it demonstrated the morphology and size had little effect on the intensity and the polarization of the SHG response, moreover, the orientations of the micro/nano-crystals were also founded. Based on the previous related research and the optical SHG properties of $NaNbO_3$ micro/nano-crystals, the non-toxic $NaNbO_3$ micro/nano-crystals may find promising applications in biological imaging, etc.